Robotica (2002) volume 20, pp. 261–268. © 2002 Cambridge University Press
DOI: 10.1017/S0263574701003988 Printed in the United Kingdom

Robotic laser welding: seam sensor and laser focal frame registration

J.P. Huissoon

Department of Mechanical Engineering, University of Waterloo, Waterloo, Ontario N2L 3G1 (Canada)

(Received in Final Form: November 12, 2001)

SUMMARY

Robotic laser welding places extreme demands on the spatial accuracy with which the robot must position the focal point of the laser with respect to the joint to be welded. The required level of accuracy is difficult to achieve in a production environment without the use of end-point sensor based control of the robot. This requires that the end-point sensor frame and welding laser frame be accurately calibrated with respect to each other, as well as with respect to the robot wrist frame. This calibration can be difficult to perform since the sensor and laser frames are virtual in the sense that these are located in space with respect to the physical hardware, and the wrist frame of the robot is often not physically accessible. This paper presents the design of a calibration system with which these frames may be precisely defined with respect to each other.

KEYWORDS: Laser welding; Robots; Seam tracking; Calibration.

1. INTRODUCTION

Robotic laser welding has become much more practical with the development of multikilowatt Nd:YAG lasers, since the light from these lasers can be delivered to the focussing optics using a flexible fibre-optic light guide. With many robots being used successfully for other welding processes, their application to laser welding would seem logical. However, the positional accuracy of the focal point required for laser welding (typically ±0.1 mm) is at the limit of most robots' static accuracy, and the dynamic accuracy is typically much worse than this. Since typical laser welding speeds often exceed 0.1 m/s, the dynamic accuracy is important.

The accuracy with which the parts to be welded are positioned in the robot workcell is clearly also critical, as are the dimensional tolerances on the parts themselves. It would be unrealistic to expect (or prohibitively expensive to implement) that the required level of accuracy (±0.1 mm) could be generally achieved in a production environment. The far better solution is to detect the actual location of the seam to be welded with respect to the focal point of the laser, and correct the robot trajectory as the weld is made. This requires the use of a seam-tracking sensor and a tracking technique such as described in references [1,2].

A seam-tracking sensor measures the position of the seam with respect to a coordinate frame associated with the sensor. Any error in seam position is transformed from the sensor coordinate frame to the tool coordinate frame. This error is then used by the robot controller to modify the tool trajectory, based on the tool transformation defined. For this to function correctly, the relative position and orientation (or pose) of the sensor frame with respect to the robot wrist frame, and the frame associated with the focal point and axis of the laser, must be precisely calibrated. This frame calibration issue is critical: if improperly calibrated, the weld will be consistently placed beside the seam, or the laser will be out of focus.

An associated issue when relying on a seam-tracking sensor to guide the robot, is the consequence of an inadvertent knock that changes the relative pose of the sensor with respect to either the welding laser or wrist frame. If this happens, the robot becomes a highly consistent scrap production machine until the error is detected and corrected. It is therefore highly desirable to be able to automatically verify the calibration at regular intervals during production. If a change in pose is detected, the system should be able to automatically compute the appropriate compensation, or warn an operator that recalibration is necessary.

Recognizing the inability of many sensors to provide complete pose measurements, Everett and Ong devised a calibration sensor that was capable of precisely detecting the position of the centre of a reference sphere.[3] By moving the sensor with respect to the reference sphere, the position where the surface of the sphere was tangent to three light paths within the sensor could be determined. Using three reference spheres arranged on a calibration fixture, the pose of the sensor frame with respect to the robot wrist frame could be obtained. A similar technique has also been described for calibrating a robotic spot-welding gun,[4] by detecting the trip point of an optical sensor with a sequence of motions of the welding gun. However, with seam-tracking laser welding, the end-of-arm sensor-tool-wrist frame combination itself must be calibrated and checked, preferably without changing the welding cell duty cycle.

This paper presents a calibration system consisting of a reference object and a laser focal point (or end-point) sensor. The reference object is designed so that a structured-light seam-tracking sensor can be used to determine uniquely the pose of a frame associated with the reference object with respect to a frame associated with the seam-tracking sensor. This enables the seam-tracking sensor frame to be calibrated with respect to the robot wrist frame.

The end-point sensor is designed so that the axis and focal point of a welding laser can be determined uniquely with respect to the frame associated with the seam-tracking sensor. The combination of these measurements enables the complete sensor-tool-wrist frame transformations to be quickly established to the level of precision required for laser welding applications.

2. SENSOR TO WRIST FRAME POSE MEASUREMENT

Determining the transformation that defines the sensor frame with respect to the wrist frame is referred to as the sensor mount registration problem. This was first addressed by Shiu and Ahmad,[5] although several other approaches for obtaining a solution have been presented by Chou & Kamel,[6] Tsai & Lenz,[7] Zhuang & Shiu,[8] and Park & Martin.[9] The problem can be generally defined by the matrix equation:

$$AX = XB \tag{1}$$

where the matrices A and B define the transformations between two positions of the wrist frame and sensor frame respectively, and X is the sought transformation defining the pose of the sensor frame with respect to the wrist frame. The procedure is fairly straightforward: the robot is moved to an initial position, say P1, and the pose of a fixed reference object with respect to the sensor is recorded. The robot is then moved to a second position, say P2, and the pose of the reference object is again recorded. The matrix A is then computed as the transformation taking P1 to P2, and the matrix B is computed as the change in pose of the reference object recorded at P1 and at P2. The only restriction on the motion from P1 to P2 is that this must comprise a rotation about some arbitrary axis.

It was shown in reference 5, that one such rotation (from P1 to P2) leaves the problem underconstrained; a second rotation about another axis (which must not be parallel nor antiparallel to the first axis of rotation) with an accompanying object pose measurement is required for the problem to be solved uniquely. Thus with two motions and three measurements, the pose of the sensor frame with respect to the wrist frame can be found. Once calibrated, it also enables a single measurement of the reference object to be used to check if the calibration is still valid and if not to be, it enables the sensor-wrist to be recomputed automatically. However, this does not require that the sensor is capable of measuring the complete pose of the reference object. When using a structured light seam-tracking sensor, the reference object must have certain characteristic features for complete pose measurement to be possible.

3. POSE MEASUREMENT USING A SEAM TRACKING SENSOR

The structured light seam-tracking sensor (or laser-profiling sensor) effectively provides a section of the surface of the workpiece. This is illustrated in Figure 1, where the sensor is positioned over a lap joint. The resulting image data is inherently two dimensional, and the problem of measuring

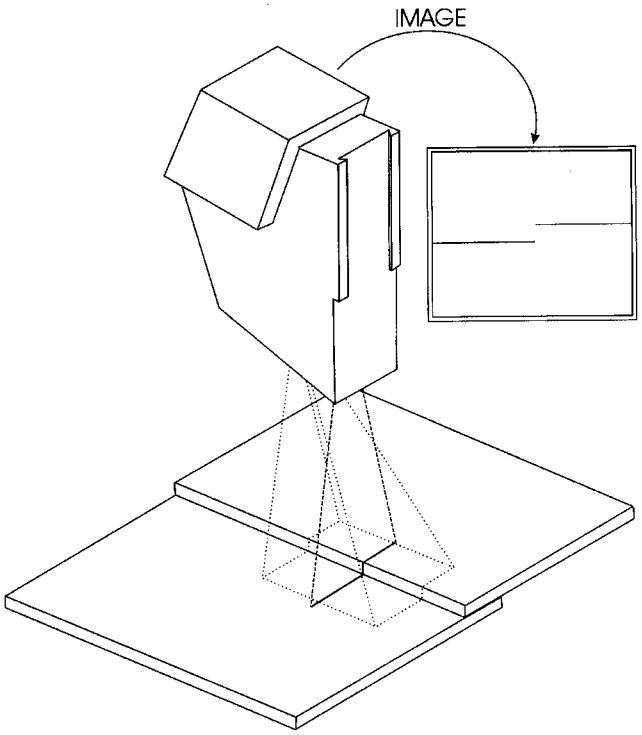

Fig. 1. Laser profiling (seam tracking) sensor viewing lap point.

the complete pose of a reference feature becomes an issue. For example, in Figure 1, rotating the sensor about the axis normal to the workpiece surface at the seam, or translating the sensor along the seam will not alter the image of the lap joint. It is therefore not generally possible to obtain complete position or orientation information of the sensor with respect to an arbitrary object or surface.

Edge features on an object appear as discontinuities in the sensor image data, and their location in the image can be determined by segmentation. A straight edge feature on a reference object occurs at the intersection of two planar surfaces on the object, and is thus defined as a straight line in 3-space. As illustrated in Figure 2, the parametric representation of a straight line can be expressed with respect to a reference coordinate frame R as:

$$P + tn \tag{2}$$

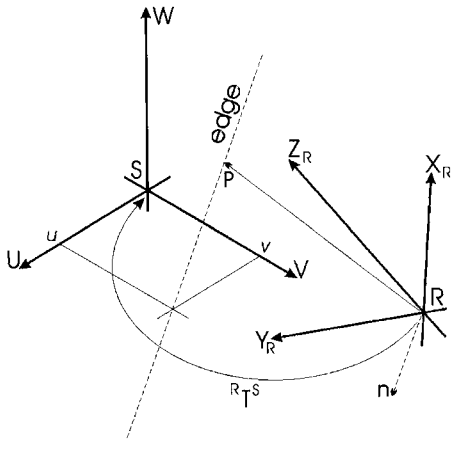

Fig. 2. Seam tracking sensor frame S and reference frame R, showing edge defined with respect to reference frame.

https://doi.org/10.1017/S0263574701003988 Published online by Cambridge University Press

where P is a vector $[P_x, P_y, P_z]^T$ from the origin of R to a point on the line, n is a unit vector $[n_x, n_y, n_z]^T$ along the line, and t is a scalar. The structured light-plane in which the sensor detects the line (or edge) feature can be defined as the UV plane of a local frame S associated with the sensor.

If the sensor frame pose is defined with respect to the reference coordinate frame R by the homogeneous transformation ${}^{R}T^{S}$

$$ {}^{R}T^{S} = \begin{bmatrix} a_{11} & a_{12} & a_{13} & a_{14} \\ a_{21} & a_{22} & a_{23} & a_{24} \\ a_{31} & a_{32} & a_{33} & a_{34} \\ 0 & 0 & 0 & 1 \end{bmatrix} \tag{3} $$

the edge feature detected in the sensor data at sensor frame S coordinates $[u, v, O]$ can be expressed in reference frame coordinates as:

$$ \begin{bmatrix} a_{11}\,a_{12}\,a_{13}\,a_{14} \\ a_{21}\,a_{22}\,a_{23}\,a_{24} \\ a_{31}\,a_{32}\,a_{33}\,a_{34} \\ 0\quad 0\quad 0\quad 1 \end{bmatrix} \times \begin{bmatrix} u \\ v \\ 0 \\ 1 \end{bmatrix} = \begin{matrix} a_{11}.u + a_{12}.v + a_{14} \quad (i) \\ a_{21}.u + a_{22}.v + a_{24} \quad (j) \\ a_{31}.u + a_{32}.v + a_{34} \quad (k) \end{matrix} \tag{4} $$

which can be equated to the parametric representation of the edge feature as:

$$ \begin{aligned} P_X + t.n_X &= a_{11}.u + a_{12}.v + a_{l4}\,(i) \\ P_Y + t.n_Y &= a_{21}.u + a_{22}.v + a_{24}\,(j) \\ P_Z + t.n_Z &= a_{31}.u + a_{32}.v + a_{34}\,(k) \end{aligned} \tag{5} $$

In addition to these three equations, three further equations that define the vectors a_{i1} and a_{i2} as being orthonormal, can be expressed as:

$$ \begin{aligned} a_{11}^{\,2} + a_{21}^{\,2} + a_{31}^{\,2} &= 1 \\ a_{12}^{\,2} + a_{22}^{\,2} + a_{32}^{\,2} &= 1 \\ a_{11}\,a_{12} + a_{21}\,a_{22} + a_{31}\,a_{32} &= 0 \end{aligned} \tag{6} $$

Thus for a single straight edge feature for which P and n are known, six equations may be formulated in 10 unknowns. If two edges can be detected on the reference object, three additional equations may be formulated, but only one additional unknown is introduced: the value of t where the second edge intersects the light plane. With three detectable edges, a set of 12 equations in 12 unknowns can be formulated. However, three of these equations (6) are nonlinear and four solutions exist. Since the objective in designing the reference object is that its pose can be determined uniquely, three detectable edge features will not suffice. Furthermore, even if the ambiguity could be resolved, the inevitable inaccuracy (measurement noise) in measuring the edge locations usually leads to problems in computing the solution. Hence, a reference object with at least four edges is desirable, although all four edges do not need to physically exist.

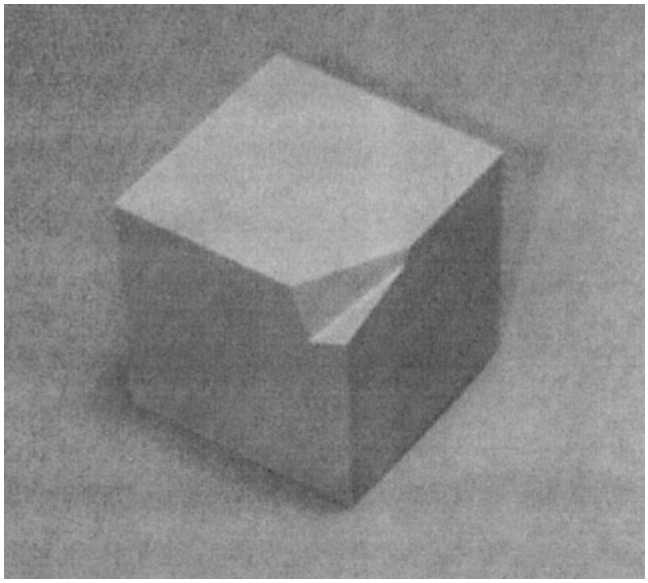

Fig. 3. Photo of reference object, showing three edges used for calibration.

Figure 3 shows a reference object, one corner of which has been machined to create three diverging reference edges. However, a fourth 'virtual' edge can be constructed at the intersection of the projection of the outermost planes. This is apparent from the structured light sensor data for an image of the object, as shown in Figure 4. The location of each of the four 'edges' with respect to the sensor can be readily calculated at the intersections of lines fitted to the data corresponding to the reference object's surfaces. An important advantage to computing the edge locations in the sensor image from the intersection of lines is that this can provide sub-pixel accuracy from least squares lines fitted to the sensor data.

Once the edge locations have been determined in the sensor coordinate frame, the pose of the reference object with respect to the sensor coordinate frame can be established. However with four edges, the problem is overconstrained, with 15 equations in 13 unknowns, although 3 of these equations (see (6) above) are non-linear. The solution adopted is to first eliminate the variable t in each set of edge equations (5), which then provides a set of 8 linear equations in 9 unknowns. This set of equations is then solved using the singular value decomposition (SVD) technique, which results in a 'least squares' line solution. The solutions along this line are then used to compute the

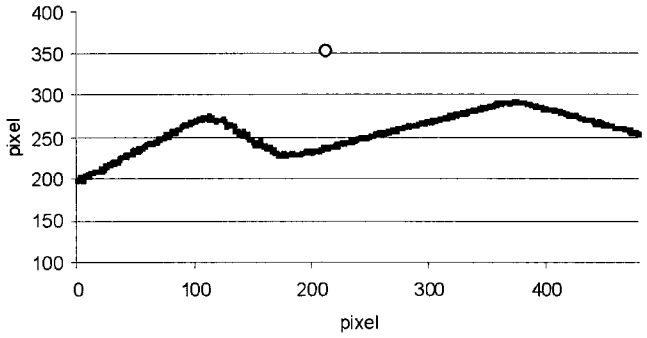

Fig. 4. Sensor image pixel data for reference object, also showing location of the virtual edge.

https://doi.org/10.1017/S0263574701003988 Published online by Cambridge University Press

sum-of-squares error (SSE) for the unit vector and orthogonalityrelationships, and the minimum of the SSE is used to identify a global least squares solution to the problem.

While this technique works very well with simulated data, it has been found to be prone to measurement noise and provides only a good estimate when actual measurement data are used. However the forward problem can also be solved: given an assumed sensor frame pose with respect to the reference object, the location of the edges in the sensor image can be predicted. Using the solution provided by the SVD algorithm as an initial estimate of the sensor pose, a multidimensional optimization technique (such as the Simplex algorithm) can be used to quickly converge to the sensor pose that provides a general least squares best fit to the measured edge locations.

4. LASER TOOL-FRAME POSE MEASUREMENT

The requirements for a reference object that enables a complete pose measurement to be made using a structured light seam-tracking sensor have been described in the previous section. This in turn enables the pose of the seam-tracking sensor to be determined with respect to the robot wrist frame, as described in section 2. With the wrist-to-sensor transformation established, the sensor-to-tool transformation is next determined, which then enables the tool transformation to be computed.

The origin of the tool frame corresponds to the focal point of the welding laser. Since the laser beam is axially symmetrical, only this axis of the tool frame and the tool frame origin need be determined. A low-power focussing-laser is normally provided to determine the focal point of the welding laser itself. This focussing-laser can be safely projected onto an etched glass plate without damaging the surface of the plate. By viewing an image of the projected focussing-laser light, the focal height can be determined as that which minimizes the diameter of the light spot in the image.[10]

A laser focal-point sensor was constructed using a CCD camera to measure the centroid location and the area of the projected focussing-laser light on an etched glass surface. This sensor is shown in Figures 5a and 5b. The CCD camera is located at one end of an aluminium tube, some 140 mm from the etched glass plate at the other end of the tube, and

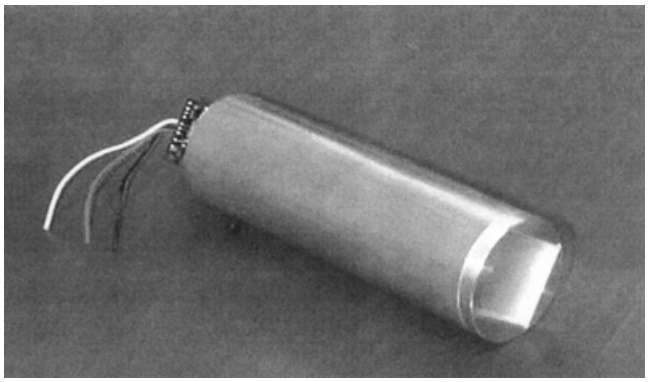

Fig. 5a. Photo of laser focal point sensor. The CCD array sensor is mounted on the circuit board just visible at the left end of the cylinder.

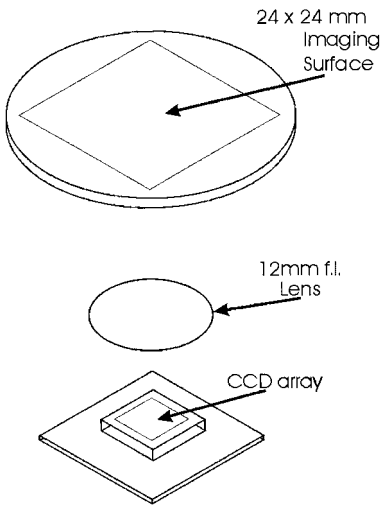

Fig. 5b. Sensor component arrangement within aluminium cylinder.

views a 15×20mm image area of the plate surface. Referring to Figure 6, a laser sensor reference frame, LS, is defined with respect to the camera. The Z_{LS} axis is parallel to the camera lens axis, the X_{LS} and Y_{LS} axes are defined with respect to the camera CCD array, and the origin of the frame is located on the etched glass imaging surface, the X_{LS} Y_{LS} plane.

The reference object previously described and the laser focal point sensor are integral components of the calibration system. The reference object is fixed in a known pose with respect to the LS frame so that the laser axis is approximately centered in the image when the reference edges are nominally centered in the field of view of the seam-tracking sensor. This arrangement depends on the design and dimensions of the fixture by which the seam-tracking sensor is attached to the laser delivery head, which in turn may be influenced by the desired angle of incidence of the laser beam on the workpiece, and the reflectivity of the workpiece surface. It is important that the transformation ${}^{R}T^{LS}$ relating the reference object frame R to the laser sensor reference frame LS is known, either from the mechanical drawings or from measurements.

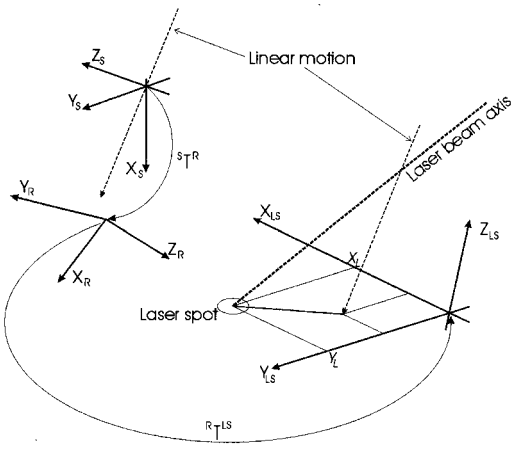

Fig. 6. Frames and transformations relating seam-tracking sensor frame S, reference object frame R, and laser sensor frame LS.

https://doi.org/10.1017/S0263574701003988 Published online by Cambridge University Press

The sensor is used by positioning the seam sensor and laser over the calibration system, as shown in Figure 7. The laser is moved in a straight line towards the imaging surface (the X_{LS}-Y_{LS} plane), starting with the laser focal point above the imaging surface and continuing until the focal point is below the imaging surface (or vice versa). A sequence of images is captured by the camera during this motion, and each is analysed to determine the area of the laser beam and its centroid location on the X_{LS}-Y_{LS} plane. As each image is captured, the position of the reference object with respect to the seam tracking sensor is also recorded. An incremental linear motion of $[\delta x\ \delta y\ \delta z]$ of the wrist frame of the robot can be measured precisely by the relative motion of the sensor frame S with respect to the reference frame R. This motion will result in the centroid of the projected laser spot moving by $[\delta x_{LS}\ \delta y_{LS}]$ across the imaging plane.

The axis of the laser beam is determined with respect to the seam-tracking sensor using a similar approach to that described by equations (2) to (5). Here the transformation ${}^{S}T^{LS}$ replaces the matrix ${}^{R}T^{S}$, the point $[u, v, O]$ is replaced by the point $[x_{LS}, y_{LS}, O]$, and the straight line described by the parametric equation is the axis of the laser beam, the parameters for which are sought. Thus for each measurement, a set of three equations can be obtained as:

$$\begin{aligned} P_X + t.n_X &= c_{11}.x_{LS} + c_{12}.y_{LS} + c_{14}\ (i) \\ P_Y + t.n_Y &= c_{21}.x_{LS} + c_{22}.y_{LS} + c_{24}\ (j) \\ P_Z + t.n_Z &= c_{31}.x_{LS} + c_{32}.y_{LS} + c_{34}\ (k) \end{aligned} \tag{7}$$

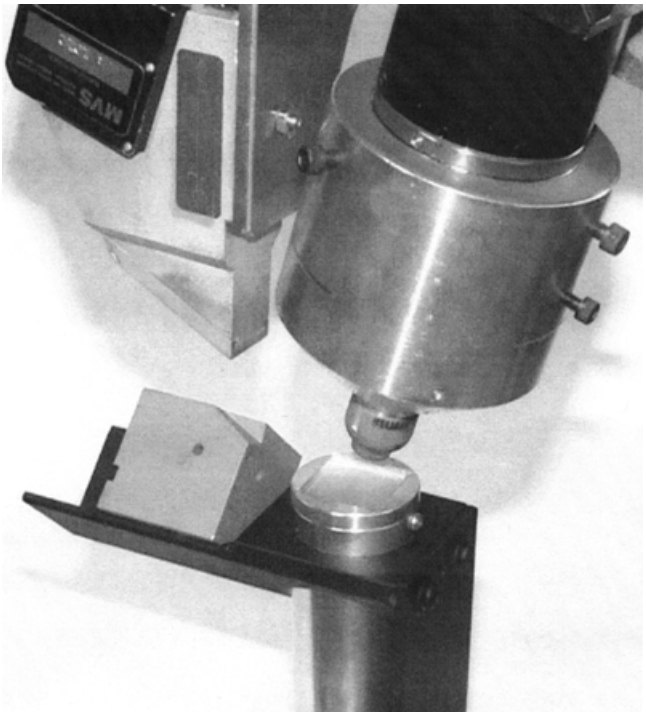

Fig. 7. Seam sensor (on left) and laser head positioned over calibration system.

where x_{LS} and y_{LS} are the measured co-ordinates of the centroid of the projected laser beam on the X_{LS}-Y_{LS} plane, $[n_x\ n_y\ n_z]^T$ is the sought unit vector along the laser beam axis, and

$$c_{ij} = \sum_{k=1}^{4} a_{ik} b_{kj}$$

in which the a_{ij} and b_{ij} are the components of the transformations ${}^{S}T^{R}$ and ${}^{R}T^{LS}$, respectively.

For any pair of measurements, subtracting the associated equations yields the following relationships for the components of the axis of the laser beam with respect to the sensor frame S:

$$\begin{aligned} t_0 n_x &= c_{11}\delta x_{LS} + c_{12}\delta y_{LS} + \delta x \\ t_0 n_y &= c_{21}\delta x_{LS} + c_{22}\delta y_{LS} + \delta y \\ t_0 n_z &= c_{31}\delta x_{LS} + c_{32}\delta y_{LS} + \delta z \end{aligned}$$

A least squares fit to the data for the sequence of measurements provides the required unit vector along the laser beam axis.

The focal point of the laser with respect to the sensor frame S is determined as the coordinate along the beam axis corresponding to the minimum area of the projected laser beam on the imaging surface. Since the focussing optics produce what could be considered as a cone of laser light, the area of the projected laser beam should vary as the square of the distance from the focal point. Thus by fitting a least squares quadratic curve to the measured beam area as a function of distance, the focal point is obtained at the minimum in the curve. The symmetry of the laser beam about its axis makes the definition of an X_L axis direction quite arbitrary, and the required laser focal frame parameters are therefore completely defined by above procedure.

5. EXPERIMENTAL RESULTS AND DISCUSSION

The accuracy with which the pose of the reference object can be measured by the seam tracking sensor, and the accuracy with which the laser focal point sensor can determine the beam axis were investigated with several experiments.

The first set of experiments was designed to investigate the accuracy with which the relative position of the reference object could be measured with respect to the seam-tracking sensor, with no change in orientation between the reference cube and the sensor. A simple test rig was constructed that enabled the reference object to be moved along a straight edge with respect to the seam-tracking sensor. The reference object was moved along the edge in 1.0 ±0.02 mm increments, and three measurements of the relative pose of the sensor with respect to the reference object were recorded at each position. The results for one of these experiments are presented in Figures 8 and 9. It is evident that the translation components (Fig. 8) conform closely to the expected linear relationship, with a standard deviation of less than 0.1 mm in the X and Z directions (i.e. in the light plane of the sensor), and 0.2 mm

https://doi.org/10.1017/S0263574701003988 Published online by Cambridge University Press

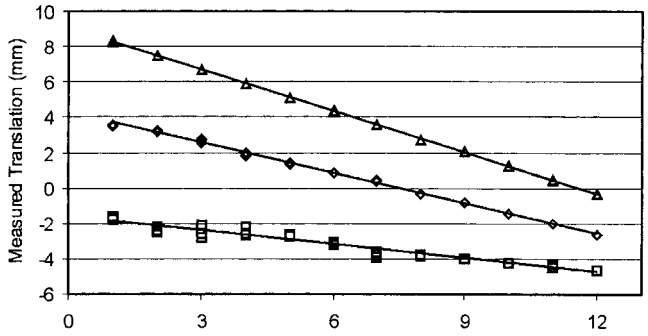

Fig. 8. Translations along X (◇), Y(□), Z(△), as reference object is moved in a straight line away from seam-tracking sensor.

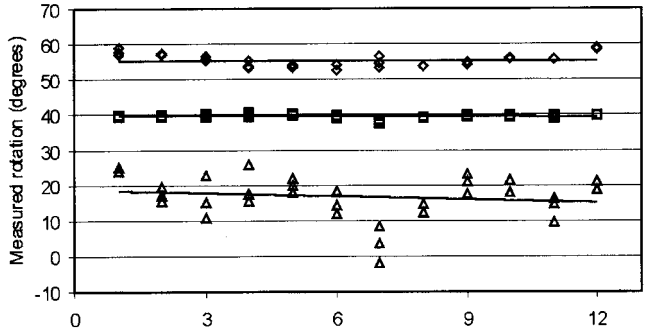

Fig. 9. Rotations Rz(◇), Ry(□), Rx(△), as reference object is moved in a straight line away from seam-tracking sensor.

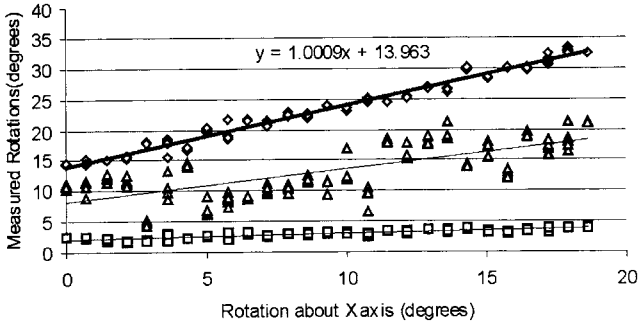

Fig. 10. Rotations Rz(◇), Ry(□), Rx(△), as reference frame axes as reference object is rotated about its X axis.

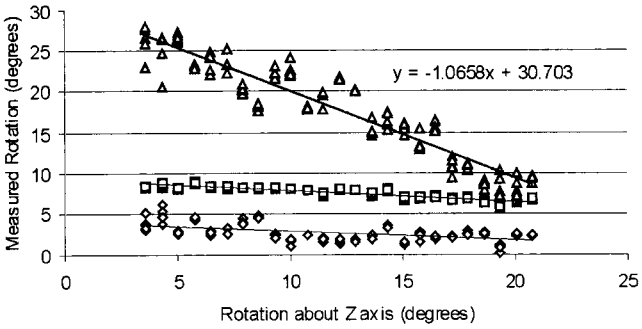

Fig. 11. Rotations Rz(◇), Ry(□), Rx(△), about reference frame axes as reference object is rotated about its Z axis.

in the Y direction. This larger variation in the Y direction measurements is due to the resolution of the sensor in measuring the divergence of the edges: the average divergence angle is about 25°, and so an incremental motion of 1 mm in the Y direction would result in a change of only 0.47 mm in the edge location in the sensor light plane. The rotational components (which should be constant) show significant variation about certain axes. Variation about the Y axis, which should be most easily measurable, is quite acceptable at a standard deviation of 0.5°. However, the measurement data about the X and Z axes are somewhat disappointing: the Z axis rotation appears to exhibit a non-linear trend, about which the variation would likely be acceptable, and the X axis rotation is clearly noisy, with variation of typically ±3° for any given reading. While the accuracy of these measurements of rotation about the X and Z axes relies on the ability of the sensor to detect very small differences in edge locations (and thus measurement noise could be expected), it is the evident trend in the data that causes most concern. Possible reasons for this are discussed later.

A second set of experiments was designed to investigate the ability to detect rotation of the reference object about its primary axes. Three holes (3.23 mm diameter) were drilled and reamed 15 mm from the face planes of the reference cube and parallel to each reference frame axis. By supporting the reference object on a length of 3.18 mm diameter drill rod passed through one of these holes, and rotating the reference object about the rod, a rotation about one reference frame axis could be achieved without incurring any rotation about the other two axes. The results of the experiments for rotations about the X and Z axis are presented in Figures 10 and 11 respectively. The data in these figures are expressed as rotations about the reference object's axes. From Figure 10 it is evident that the rotation about the X axis is accurately measured, with a standard deviation of 0.83°. However, rotations about the Y and Z axes are also evident, neither of which should be present. Moreover, these rotations exhibit a definite trend, and cannot be attributed to measurement noise. While the slope of the trend for the observed Y axis rotation is less than 10% of that for the axis about which the rotation actually occurred, the slope of the trend for the Z axis rotation is almost 60% of that about the X axis. This is a difficult result to explain in terms of error in rotation that could have been induced by misalignment in the test setup: since the axis of rotation was fixed with respect to the sensor, the only possible cause could have been misalignment of the holes drilled in the reference cube with respect to the reference cube faces, and these were measured to be accurate to better than 0.05°. Figure ll shows the results when the reference cube is rotated about its Z axis. The measured Z axis rotation is seen to be quite accurate although noisy, with a standard deviation of 2.04°, but again, rotations about the other axes are observed, which should not have occurred. While these rotations are less significant than those measured when rotating about the X axis, there is again a definite trend in the Y axis rotation, as well as about 3° of noise in the X axis measurements.

The most likely explanation for the observed trends in rotations about axes about which there should have been no rotation, is that these result from distortion in the sensor optics. It is well recognised that optical sensors can suffer from "barrel" distortion due to the lenses used.[11,12] For the sensor used in this work, the distance measured to a planar

https://doi.org/10.1017/S0263574701003988 Published online by Cambridge University Press

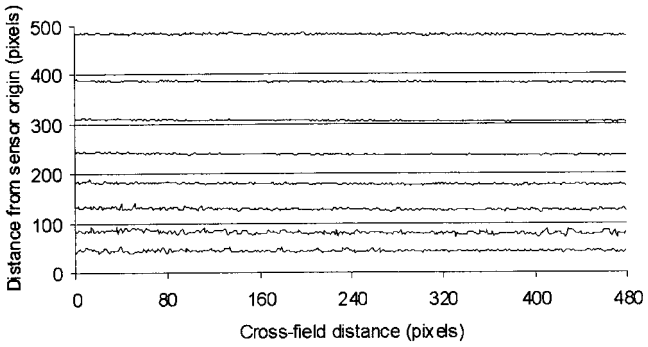

Fig. 12. Sensor data for a flat surface perpendicular to sensor Y axis as the surface is moved along the Y axis in 1.5 mm increments (8 individual data sets shown).

surface normal to the sensor Y axis varies slightly across the field of view, and as a function of distance from the sensor, as shown in Figure 12. While the measured error is generally within one or two pixels, there are areas at the edges of the field of view where this increases to more than 6 pixels. A look-up-table of values was used to compensate for this distortion, and reduced the measurement error in the sensor Y axis direction to within 1 pixel across the field of view. However, the crossfield distortion was not compensated for, and this is the only plausible explanation for the trends observed in the data shown in Figures 9 to 11. This highlights the importance of precise sensor calibration in applications such as this, where a few pixels distortion is almost certainly the culprit in producing otherwise puzzling results.

A third set of experiments was designed to investigate the premise that the laser beam axis could be defined using the centroid of the projected laser beam as detected by the laser focal-point sensor, when the laser was moved in a straight line with respect to the sensor. The laser delivery head (focussing optics) was mounted over the table of a milling machine, with the laser axis inclined at 15° to the vertical. The sensor was attached to the table itself, and positioned so that the focussing laser was approximately centered on the etched glass window. The table was raised and lowered manually in 1.27 mm increments, and an image from the CCD camera was recorded at each position. A sequence of 4 representative images, taken 2.54 mm apart, is shown in Figure 13. Note that main spot on which the calculations are based is to the left, and that the "shadow" spot to the right occurs due to partial reflection off the back surface of the mirror in the optical system used.

Figure 14 shows the X and Y location of the centroid of the laser spot as the table elevation is changed in 1.27 mm

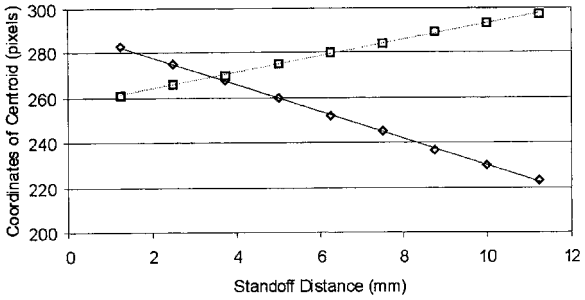

Fig. 14. Measured laser spot centroid location as laser is moved in a sraight line towards sensor screen, ◇= X, □= Y.

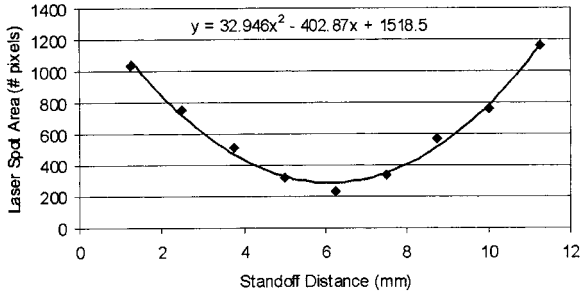

Fig. 15. Measured laser spot area as laser is moved in a straight line towards sensor screen. The focal point is at the minimum in the curve.

increments. Excellent co-linearity of the data points is evident, a least squares straight line through these data yielding a standard deviation of 0.02 mm. The beam axis angle with respect to the sensor is calculated as 14.52°. Figure 15 shows the laser spot area as a function of table elevation, with a least squares quadratic curve fitted to the data. The focal point is just to the left of the minimum data point, and can certainly be estimated to within +0.2 mm, which is acceptable for this welding process.

6. CONCLUSIONS

A sensing system and measurement technique have been described with which the coordinate frames associated with a seam-tracking sensor, a welding laser, and the robot wrist frame may be experimentally established. It has been shown that a reference object with respect to which a structured light sensor can determine its relative pose, requires at least four detectable edge features, and an easily manufacturable design that satisfies these requirements has been presented. The accuracy with which the position of the sensor can be measured with respect to the reference object is acceptable for laser welding, assuming that the sensor has been accurately calibrated. By coupling the reference object with

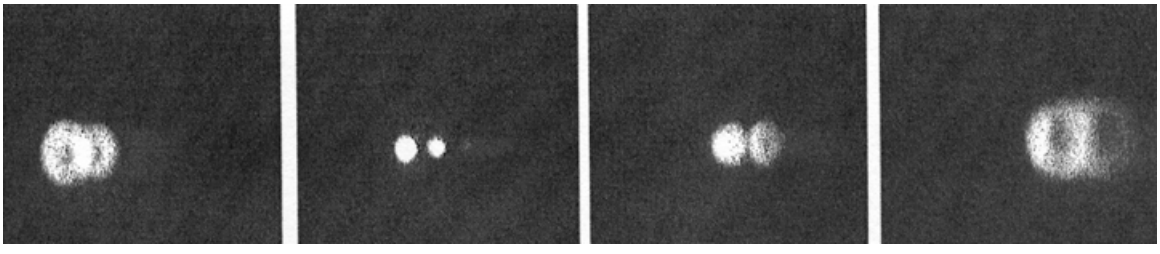

Fig. 13. Sequence of images of laser spot as the laser is moved towards the screen in 2.5 mm increments.

https://doi.org/10.1017/S0263574701003988 Published online by Cambridge University Press

an active sensor that can detect the relative location of the laser beam, the laser focal point and beam axis with respect to the seam tracking sensor can be determined, thus greatly simplifying an otherwise difficult calibration task.

ACKNOWLEDGEMENTS

This research has been supported by the Institute for Robotics and Intelligent Systems (IRIS) and Materials and Manufacturing Ontario (MMO).

References

1. L.J. Zana, "Automatic seam tracker and real-time error cumulative control system for an industrial robot," *US patent 4,952,772* (1990).
2. J.P. Huissoon and D.L. Strauss, "Sensor Based Control of Industrial Robots," *Proc. IMC-12*, (1995) pp. 13–20.
3. L.J Everettt and L.E. Ong, "Solving the Generalized Sensor-Mount Registration Proble," *Proc. ASME Winter Annual Mtg.* (1991) **DSC-Vol. 29**, pp. 7-14.
4. H.F. Thorne, "Tool center point calibration apparatus and method," *US patent 5,457,367* (1995).
5. Y.C. Shiu and S. Ahmad, "Calibration of Wrist-Mounted Robotic Sensors by Solving Homogeneous Transform Equations of the Form AX=XB," *IEEE Trans. Robotics & Automation,* **5**(1), 16–29 (1989).
6. J.C.K. Chou and M. Kamel, "Quaternions Approach to Solve the Kinematic Equation of Rotation AaAx = AxAb of a Sensor Mounted Robotic Manipulator," *Proc. 1988 IEEE Int. Conf. Robotics & Automation,* Philadelphia, PA. (1988) pp. 656–662.
7. R.Y. Tsai and R.K. Lenz, "A New Technique for Fully Autonomous and Efficient 3D Robotics Hand/Eye Calibration," *IEEE Trans. Robotics & Automation,* **5**(3), 345-357 (1989).
8. H. Zhuang and Y.C. Shiu, "A Noise-Tolerant Algorithm for Robotic Hand-Eye Calibration with or without Orientation measurement," *IEEE Trans Systems, Man & Cybernetics,* **23**(4), 1168–1175 (1993).
9. F.C. Park and B.J. Martin, "Robot Sensor Calibration: Solving AX equals XB on the Euclidean Group," *IEEE Trans. Robotics &Automation* **10**(5), 717–721 (1994).
10. C. Roundy, "Propagation factor quantifies laser beam performance," *Laser Focus World,***35**(12), 119–122 (1999).
11. R.Y. Tsai, "A Versatile Camera Calibration Technique for High-Accuracy 3D Machine Vision Metrology using Off-the-Shelf TV Cameras and Lenses," *IEEE Trans Robotics & Automation,* **3**(4), 323–344 (1987).
12. J. Weng, P. Cohen and M. Herniou, "Camera Calibration with Distortion Models and Accuracy Evaluation," *IEEE Trans Pattern Analysis & Machine Intell.,* **14**(10), 965–980 (1992).